

# Submillimeter Imaging of NGC 891 with SHARC

E. Serabyn, D.C. Lis, C.D. Dowell, D.J. Benford, T.R. Hunter

*Caltech 320-47, Pasadena, CA 91125*

M. Trehwella

*IPAC, Caltech 100-22, Pasadena, CA 91125*

S.H. Moseley

*NASA-Goddard Space Flight Center, Greenbelt, MD 20771*

**Abstract.** The advent of submillimeter wavelength array cameras operating on large ground-based telescopes is revolutionizing imaging at these wavelengths, enabling high-resolution submillimeter surveys of dust emission in star-forming regions and galaxies. Here we present a recent  $350\ \mu\text{m}$  image of the edge-on galaxy NGC 891, which was obtained with the Submillimeter High Angular Resolution Camera (SHARC) at the Caltech Submillimeter Observatory (CSO). We find that high resolution submillimeter data is a vital complement to shorter wavelength satellite data, which enables a reliable separation of the cold dust component seen at millimeter wavelengths from the warmer component which dominates the far-infrared (FIR) luminosity.

## 1. Introduction

The recently developed submillimeter wavelength camera SHARC (Wang et al. 1996) has established the viability of long-wave imaging cameras (to about  $500\ \mu\text{m}$ ) which are based on the short-wave prescription of illuminating planar detector arrays with geometrically defined beams. Wide-field, high-resolution imaging at wavelengths just longward of the FIR regime accessible only from space-based platforms then becomes possible. Combined also with even longer wavelength submillimeter and millimeter wave data, the accurate delineation of dust emission spectra in galaxies and star-forming regions then becomes viable. Specifically,  $350\ \mu\text{m}$  data is vital to the determination of the properties of cold dust (5-20 K) because this wavelength lies near the peak emission wavelength for such dust, and so allows for a much more accurate assessment of dust parameters than can be had solely from distant longer or shorter wavelength observations.

Herein we use our  $350\ \mu\text{m}$  SHARC mapping results together with HIRES processed IRAS maps and published 1.3 mm data to constrain the properties of the dust emission in the edge-on galaxy NGC 891, an oft-cited analog to our own Milky Way. Fig. 1 presents our  $350\ \mu\text{m}$  map, acquired in Jan. 1998. Morphologically it is similar to the  $1300\ \mu\text{m}$  map of Guélin et al. (1993): three peaks are resolved along the plane of the galaxy, including the nucleus and a peak to either side attributable to the star-formation ring. The peak flux from the nucleus is  $5.6 \pm 0.55$  Jy in a  $12''$  beam, and the integrated flux in our map is 117 Jy. Furthermore, the dust layer is clearly resolved in the vertical direction, and we derive a FWHM thickness for the dust layer of  $900 \pm 100$  pc (averaged across the three main peaks).

In order to constrain the temperatures and emissivity law applicable to the dust in NGC 891, we used HIRES processed IRAS images of the galaxy together with our  $350\ \mu\text{m}$  image and the  $1300\ \mu\text{m}$  image. The angular resolution of the  $60\ \mu\text{m}$  IRAS image ( $\sim 64'' \times 45''$  at a  $-28^\circ$  position angle) is sufficient to resolve several points along the major axis of the galaxy. All the remaining images were convolved to the angular resolution of the  $60\ \mu\text{m}$  image. Since the angular resolution of the  $100\ \mu\text{m}$  image ( $\sim 100'' \times 82''$ ) was too low to be included directly in the analysis, we assumed

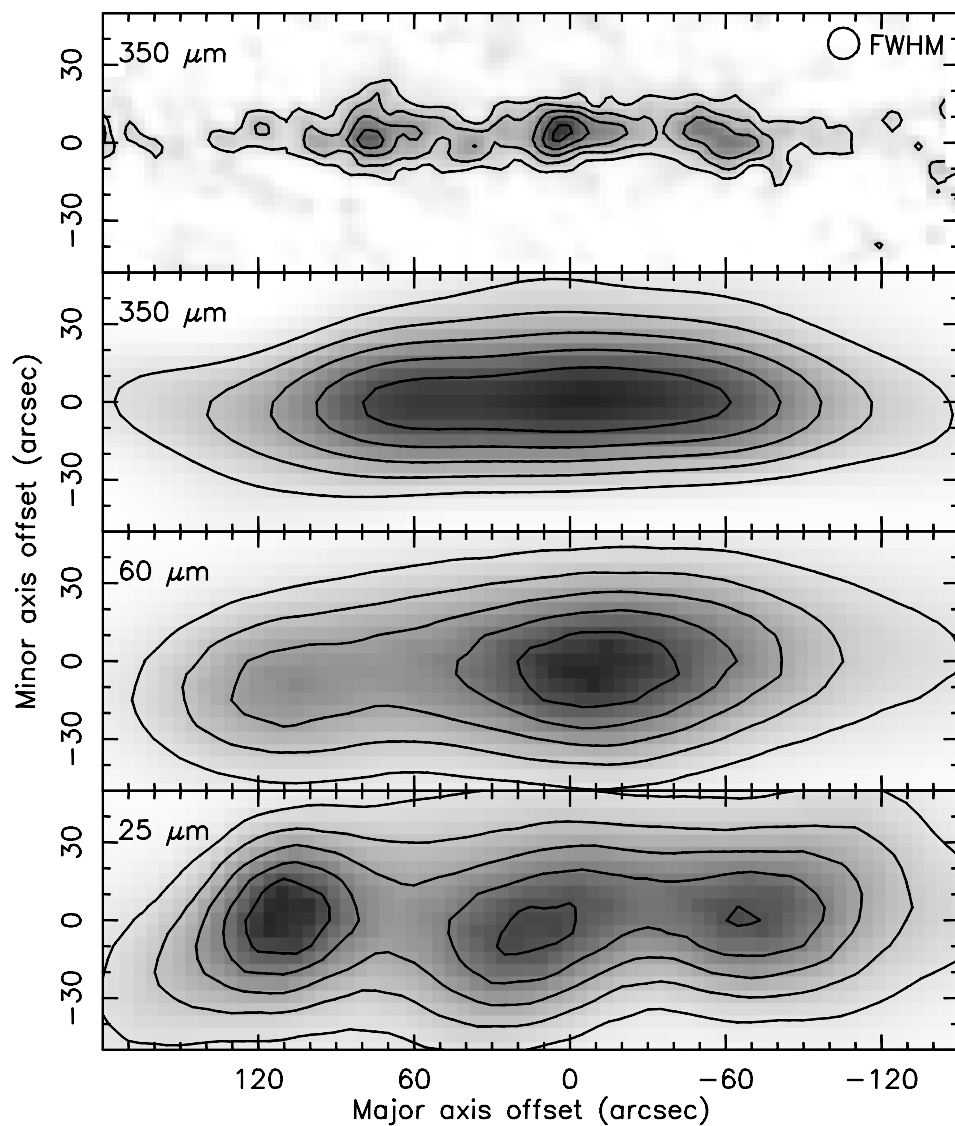


Figure 1. Submillimeter and FIR maps of NGC 891. Top panel: SHARC  $350\ \mu\text{m}$  image of NGC 891, at a resolution of  $12''$ . The peak flux on the nucleus is  $5.6\ \text{Jy}$ , and the rms noise in the map is  $0.55\ \text{Jy}$ . The image is rotated such that its major axis is horizontal, and positive offsets along the major axis are to the northeast. Second through fourth panels: Our  $350\ \mu\text{m}$  data and the IRAS HIRES data convolved to the resolution of the IRAS  $60\ \mu\text{m}$  map ( $64 \times 45''$  at a  $-28^\circ$  position angle). The peak fluxes in the 3 lower maps are  $419$ ,  $201$ , and  $15.7\ \text{MJy/sr}$ . The contours are all 25,40,55,70, and 85% of the peak values.

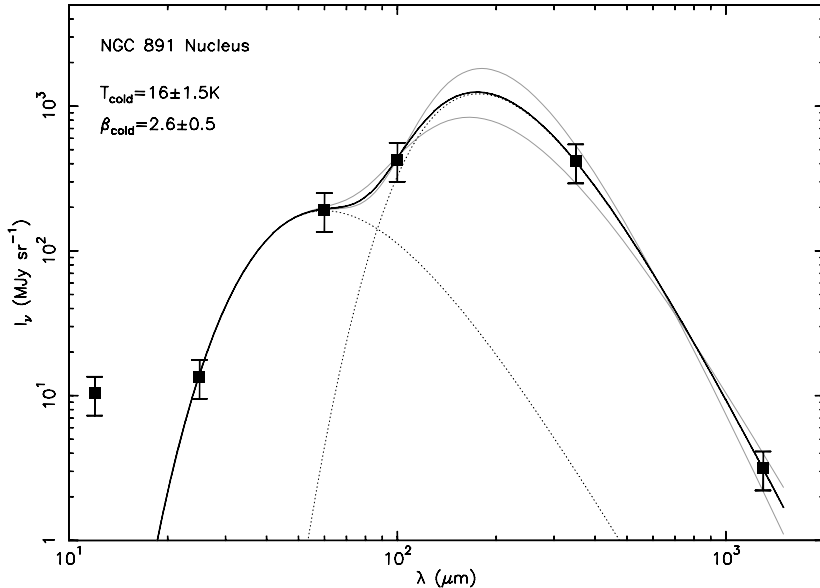


Figure 2. Spectral energy distribution for the nucleus of NGC 891, at a resolution of  $45'' \times 60''$  (black squares). Together with our  $350 \mu\text{m}$  point and the IRAS HIRES results, the  $1300 \mu\text{m}$  point of Guélin et al. (1993) is shown. The error bars correspond to an absolute calibration uncertainty of 30%. The solid curve gives the best fit two component model, with the two individual components given as dashed curves. Bounding curves to estimate error bars are given in light grey.

a constant  $100/60 \mu\text{m}$  flux ratio of 0.45 corresponding to the nucleus of the galaxy (this ratio varies only slightly across the galaxy, between  $\sim 0.4$  and 0.45).

Figure 2 shows the observed continuum spectrum toward the center of NGC891. We have modeled the observed spectrum as a sum of two modified blackbody functions (e.g. Lis & Menten 1998). We ignored the  $12 \mu\text{m}$  IRAS data point since the emission at this wavelength is strongly affected by transiently heated small dust grains. First we assumed that the  $25 \mu\text{m}$  and  $60 \mu\text{m}$  emission originates in a ‘warm’ dust component with a grain emissivity frequency exponent of  $\beta = 2$ . The dust temperature and the  $100 \mu\text{m}$  optical depth of this component were free parameters in the fit, along with the temperature,  $100 \mu\text{m}$  optical depth, and  $\beta$  for the ‘cold’ dust component, which dominates the emission at  $\lambda \gtrsim 100 \mu\text{m}$ . The parameters of the cold component are not sensitive to the assumed value of  $\beta$  for the warm component. The best fit model to the observed spectrum is shown as a solid black line in Figure 2, along with the spectra of the two individual components and a pair of limiting curves. The best fit parameters for the cold component are  $T_d = 16 \pm 2 \text{ K}$ ,  $\beta = 2.6 \pm 0.5$  (the error bars allow both for uncertainties at a given location and for variations across the three peaks), and  $\tau_{100} = 2.0$  (to a factor of 2). The resultant temperature of the warm component is  $\sim 50 \text{ K}$  (if the  $25 \mu\text{m}$  point is assumed to also arise from transiently heated grains, the temperature of the warm component can be as low as  $29 \text{ K}$ , and this results in a cold component temperature lower by a few K) and its optical depth (and mass) is a small fraction ( $\sim 3 \times 10^{-4}$ ) of the total. Similar fits obtained at several positions along the major axis of the galaxy show that the parameters describing the cold component show little variation, with cold component temperatures varying between  $15$  and  $16 \text{ K}$ , the best value of  $\beta$  between  $2.35$  and  $2.65$ , and the  $100 \mu\text{m}$  optical depth varying by about a factor of 2 for the three peaks.

To model long-wave galactic dust emission, at least 6 parameters are generally required: temperatures, long-wave opacity exponents, and reference frequency opacities for each of 2 temperature components. Measurement of these parameters has heretofore been quite difficult because of the largely inaccessible region between the longest ( $100 \mu\text{m}$ ) IRAS waveband and the millimeter regime. In particular, for dust cold enough to show peak emission in the submillimeter, these parameters are necessarily poorly defined, resulting in the need to simply assign values to a subset of the parameters, such as the temperatures involved (e.g. Guélin et al. 1993). More insidiously, attempts

to bridge the submillimeter spectral gap when a spectral peak is present therein necessarily results in a significant underestimate of the emissivity spectral index,  $\beta$ , for the coldest component. However, the addition of intermediate frequency data closer to the spectral peak allows the model parameters to be disentangled to a much greater extent. Indeed, it is precisely this effect which leads to our rather high value for  $\beta$ : with a well determined cold-component temperature of only 16 K, the only way to generate the large flux increase seen between 1.3 and 0.35 mm is with a large  $\beta$ . Thus, the intermediate frequency data at 350  $\mu\text{m}$  not only allows for a very well constrained cold-component temperature, but also for a much more reliable emissivity slope estimate. However, the ramifications also extend beyond the coldest dust component, because if a substantial fraction of the 100  $\mu\text{m}$  flux also arises in such a cold component, simple 100/60  $\mu\text{m}$  color temperatures become very misleading indicators for the warmer component.

## References

- Wang, N. et al. 1996, *Applied Optics*, 35, 6629  
Guélin, M. et al. 1993, *A&A*, 279, L37  
Lis, D.C. & Menten, K.M. 1998, *ApJ*, 507, in press